# A Novel Test and Calibration Method for Digital Signals of Relay Protection Test Equipment for Intelligent Substation Based on FPGA

Yan Huang, Hadi Nabipour Afrouzi, Hieng Tiong Su, Yuan Ping, Ismat Hijazin, Yangtao Xu, and Ke Yan

***Abstract*—With the widespread adoption of digital equipment in intelligent substations, testing digital signals in power systems has become an important role for relay protection test equipment. Testing and calibrating digital signals require high accuracy. However, existing methods have low precision, cannot be calibrated at full range for all indexes, and have complex configuration, making them unsuitable for routine calibration work. To solve the above problems, a novel calibration method is designed and implemented using field programmable gate array (FPGA) to achieve accurate input and output time control. Accurate calibration relies on multiple forms of traceability including theoretical value traceability based on waveform comparison, time scale value traceability based on accurate time stamps, and algorithm traceability based on typical algorithms. Compared with other existing methods, the proposed approach reduces the mean absolute error of action time and time measurement by 92.88%, effectively addressing a key industry challenge and offering a valuable reference for further research, application, and standardization.**

***Index Terms*—Relay protection test equipment, digital signal, calibration, field programmable gate array.**

Received: January 30, 2025
Accepted: October 28, 2025
Published Online: January 1, 2026

Yan Huang is with the Faculty of Engineering, Computing and Science, Swinburne University of Technology Sarawak Campus, Kuching 93350, Malaysia; and also with the School of Engineering, Swinburne University of Technology Hawthorn Campus, Hawthorn 3122, Australia (e-mail: 104369307@student.swin.edu.au).

Hadi Nabipour Afrouzi is with the College of Engineering, Faculty of Computing, Engineering and the Built Environment, Birmingham City University, Birmingham B4 7XG, UK (e-mail: Hadi.nabipourafrouzi@bcu.ac.uk).

Hieng Tiong Su is with the Faculty of Engineering, Computing and Science, Swinburne University of Technology Sarawak Campus, Kuching 93350, Malaysia (e-mail: hsu@swinburne.edu.my).

Yuan Ping (corresponding author) is with the School of Information Engineering, Xuchang University, Xuchang 461000, China (e-mail: pingyuan@xcu.edu.cn).

Ismat Hijazin is with the School of Engineering, Swinburne University of Technology Hawthorn Campus, Hawthorn 3122, Australia (e-mail: ihijazin@swin.edu.au).

Yangtao Xu (corresponding author) and Ke Yan are with the Xuchang KETOP Testing Research Institute Co., Ltd., Xuchang 461000, China (e-mail: xuyangtao@ketop.cn; yanke@ketop.cn).

DOI: 10.23919/PCMP.2024.000425

## I. Introduction

With the advancement of smart grids and the adoption of IEC 61850, power systems worldwide are entering the digital age. The use of digital devices and testing equipment has increased significantly, accompanied by higher demands for accuracy [1], [2].

Digital signals in power systems, such as sampled value signals, consist of discrete sampling points at a defined sampling rate [3]. Macroscopically, these signals exhibit effective amplitude and phase characteristics similar to analog signals. Microscopically, however, each individual sampling point within the waveform possesses its own amplitude and phase. When the distribution of the sampling points deviates from the ideal state, errors will be generated [4]. When the errors at the sampling points are large, the digital waveform will be distorted. Abnormalities in digital signal accuracy are not uncommon, particularly as equipment ages and failure rates increase. Under such conditions, the accuracy of digital signals generated by relay protection test equipment can no longer be guaranteed.

Time measurement and time control are two important indexes of electric power equipment, especially for relay protection test equipment. They are based on different kinds of digital signals and responsible for accurately testing the response time or action time of relay protection or other electric power equipment [3]. They mainly include digital signals such as sampled value (SV) and generic object oriented substation event (GOOSE), and contact signals [3]. In order to ensure the accuracy of time measurement, it is necessary to calibrate the equipment regularly according to the related standards. For instance, standard requirements for IEC 60255-151-2009, DL/T 1501-2016, DL/T 1944-2018, DL/T 2646-2023 and NB/T 11216-2023 show that the time measurement accuracy of relay protection test equipment needs to be higher than 100 μs [5]–[9].

Digital signals and operations such as time measurement based on digital signals are widely used in relay protection test equipment and have high accuracy requirements [10]. However, at present, due to the lack of closed-loop and standardized calibration method, electric power manufacturers and organizations need to use a variety of equipment including network recorder and assist relay protection device to build temporary calibration systems, which usually rely on the recorder and often introduce errors [11]. Moreover, there are still gaps in experimental verification methods for calibrating system errors. Some laboratories use comparative experiments to indirectly verify calibrating device errors, though this approach lacks sufficient accuracy. To address these challenges, this paper introduces a novel calibration method for assessing the digital signal accuracy of relay protection test equipment and validates its effectiveness through experimental verification.

The remainder of this paper is organized as follows. Section II presents the analysis of existing methods, while Section III discusses the design of the novel calibration system. Section IV demonstrates the key technologies of the novel method. In Section V, the performance analysis is presented, and Section VI presents the main conclusions of the paper.

## II. Analysis of Existing Methods

### *A. Existing Calibration Methods for Digital Signals Accuracy*

The accuracy of digital signals in power systems primarily includes parameters such as amplitude, phase, dispersion, delay time, synchronization. Industry practices for testing and calibration of these parameters lack standardization and are generally categorized into the following two main approaches.

*1) Digital-to-analog Conversion Method*

Digital-to-analog conversion systems convert digital signals to analog signals. Amplitude and phase errors of the measured signals are evaluated using analog signal traceability theory with established testing and calibrating methods. This approach is adopted by some calibration laboratories. However, it lacks scientific rigor, as it neglects the inherent characteristics of digital signals. Moreover, it only allows for the calibration of amplitude and phase accuracy, leaving other key parameters and indicators unaddressed [11].

*2) Network Recorder Method*

The second method utilizes network recorders to analyze the indicators of digital signals [7]. This method is adopted by many test institutions and enterprises, but the analysis of the digital signals by network recorders must be carried out in non-real-time environments after capturing the signals. Its selection of time window and sampling points is significantly affected by human operation, resulting in high uncertainty. At the same time, it is inefficient to manually check the results one by one and calculate the errors. In particular, this method cannot perform comprehensive time-window analysis, statistical evaluation, or visualization of the instantaneous values at each sampling point, making it prone to missing transient accuracy distortions. In addition, the time scale accuracy of the network recorder is low (1 μs), which is lower than the accuracy and index requirements of relay protection test equipment, bringing uncertainty to the calibration of digital signal time-related indicators. In addition, the degree of automation of this method is relatively low, and the proportion of manual operation and manual calculation is large, making is prone to measurement errors. For more complex time measurement operations, the accuracy requirement of the calibration system is higher due to the combination of different kinds of digital signals.

### *B. Existing Calibration Method for Combined Digital Signals*

For the calibration of different signal combinations, this paper refers to the requirements of relay protection test equipment for time measurement accuracy test. There are six different types of time measurement, which are combinations of three different signals (SV, GOOSE and contact signals). According to the standard requirements in DL/T 1501-2016 “Technical Specifications of Digital Test Equipment for Relay Protection”, DL/T 1944-2018 “Technical Specifications of Handheld Optical Digital Signal Test Equipment in Smart Substation”, DL/T 2646-2023 “Technical Specifications for Digital-analog Integrated Relay Protection Test Device” and NB/T 11216-2023 “Calibration Specification of Digital Signal Test Device for Intelligent Substation”, the time measurement accuracy of relay protection test equipment needs to be higher than 100 μs when the time measurement range is between 1 ms and 100 ms ($1\,\text{ms} < t \leqslant 100\,\text{ms}$), whereas the time measurement accuracy needs to be better than $\pm 0.1$ % when the time measurement range is between 100 ms and 99 999 ms ($100\,\text{ms} < t \leqslant 99\,999\,\text{ms}$) [6]–[8]. The accuracy of the calibration system should be 2 to 10 times higher than the equipment under test. So the accuracy of calibration should be better than 50 μs to 10 μs. Therefore, if the accuracy of the novel calibration method can be better than 10 μs, it will fully meet the calibration requirements.

The existing calibration method for combined digital signals is shown in Fig. 1. As seen, digital relay protection test equipment inputs SV, GOOSE, or contact signal to relay protection device or other electric power equipment. Upon receiving these signals, the relay protection device processes them according to its functional logic, and then outputs corresponding SV, GOOSE or contact signal, which are subsequently fed back to the digital relay protection test equipment. The digital relay protection test equipment calculates the time difference $\Delta T_1$ between the output signal and the

access signal as a measurement value of the corresponding action time of the relay protection device. The network recorder device has the ability to access and time mark multiple SV, GOOSE, and contact signals. During the test, the network recorder device, as a third-party monitoring device, connects the outputs of the relay protection test equipment and relay protection device, and marks the time. The time difference $\Delta T_2$ between the output signals of the relay protection test equipment and relay protection device can be calculated using the time marker of the recorder and analyzer device, as the actual value of the corresponding action time. The measurement error of $\Delta T = \Delta T_1 - \Delta T_2$ is calculated as the error of the time measurement of relay protection test equipment [11]. The accuracy of existing calibration system is 30.423 μs, which is one-third of the required accuracy of the equipment under test.

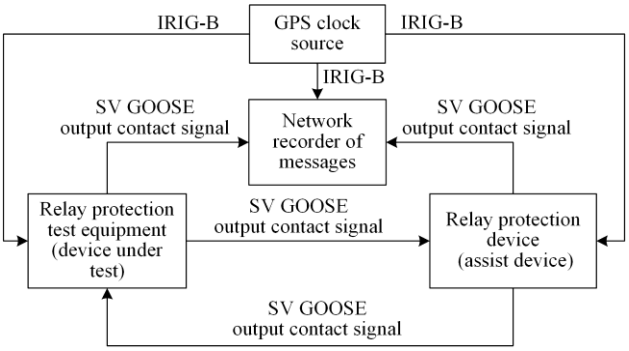


Fig. 1. Existing calibration system diagram.

### C. Drawbacks of Current Calibration Method

The existing calibration methods mainly have the following drawbacks.

*1) Low Precision*

Calibration accuracy cannot be effectively controlled, as some methods rely entirely on external devices such as network recorder or relay protection device. The network recorder and relay protection device used in calibration system are limited by their own performance, and the accuracy of the action time is relatively low (millisecond level). In addition, their fluctuation is large, which affects the measurement error of calibration, increases the difficulty of analysis and reduces the accuracy of calibration.

*2) Limited Range*

Existing methods for digital signal accuracy can only calibrate amplitude and phase, but cannot directly calibrate dispersion, delay time, synchronization and other related parameters. Regarding time measurements, the action time of the relay protection device is fixed and cannot be adjusted, making it impossible to simulate the full range of time delays (from 1 ms to 100 s) [7].

*3) Complex Configuration*

Building a temporary calibration system requires multiple types of equipment, and configuring the network recorder and relay protection device is both complex and time-consuming. A high proportion of manual operation and calculation is required, thereby increasing the likelihood of measurement errors.

## III. Design Of the Novel Calibration System

The objective of this study is to design a system to achieve high precision calibration for digital signals of relay protection test equipment. Due to its superior anti-interference capability and processing speed compared to microcontrollers, field programmable gate array (FPGA) devices can be used to perform frequency modulation and phase locking with an IRIG-B signal source. It can achieve high-precision adjustment of internal clock and provide accurate time beat to each module [12], [13].

The software and hardware components are designed to achieve the full range for all the indexes. Each of the interaction layer, logic layer and driver layer is composed of various independent functional modules. A professional and integrated calibration equipment is developed to simplify the calibration system. The novel calibration equipment presented in this study includes a high performance data processing module, a clock and synchronization module, a fast in/out module, a message receiving/sending module, a man-machine interface and a configuration module.

### A. Novel System Framework

The novel calibration system framework is shown in Fig. 2. The system includes: a novel digital signal calibration device, a digital signal output device (relay protection test equipment), and a GPS clock source. The GPS clock source provides time synchronization signals for the system [14], the relay protection test equipment outputs digital signals, and the novel calibration system detects and calibrates the digital signals. For example, the relay protection test equipment outputs SV, FT3, GOOSE or contact signals to the novel calibration system, which outputs feedback signals to the relay protection test equipment after a setting time delay (i.e., operation time).

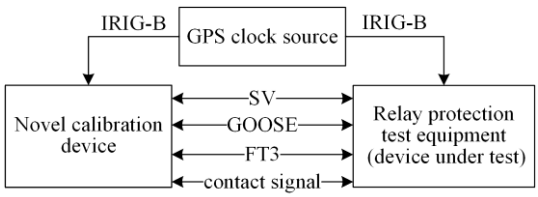


Fig. 2. Framework of novel calibration system.

### B. Novel Hardware Design

As shown in Fig. 3, the novel calibration system's hardware structure includes a configuration module, a message receiving module, a data processing module, and a message sending module [15].

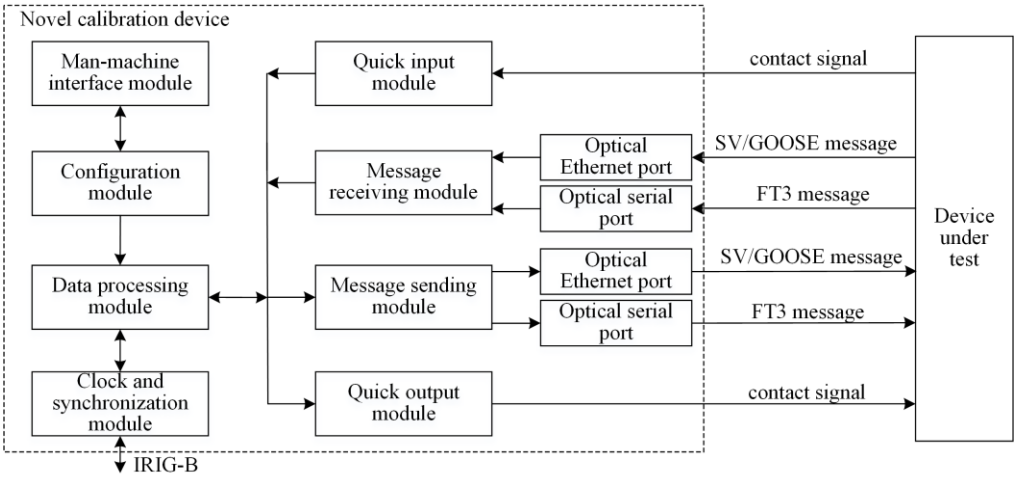


Fig. 3. Hardware design diagram of the novel calibration system.

*1) The Configuration Module*

The configuration module sets parameters for SV, FT3 and GOOSE signals, as well as contact on/off configurations. It also allows customization of settings such as the delay time between the output and input signals, as required [16].

*2) The Message Receiving Module*

The message receiving module collects the SV and GOOSE signals from the device under test, accurately marks them and sends them to the data processing module [17]. The fast access module collects the output connect signals of the device under test and sends them to the data processing module after accurately marking the time mark.

*3) The Data Processing Module*

The data processing module analyzes the incoming and outgoing signals of SV, GOOSE or contact signals. For example, it analyzes the input time of the signals, and calculates the sending time of the incoming and outgoing signals of SV, GOOSE or contact signals according to the configured delay time [18]. Then the signal sending time is sent to the message sending module.

*4) The Message Sending Module*

The message sending module sends SV, GOOSE or contact signals according to the configured network port, delay time, sending time and other configuration. Configuration and input/output display diagram of the proposed novel system is shown in Fig. 4.

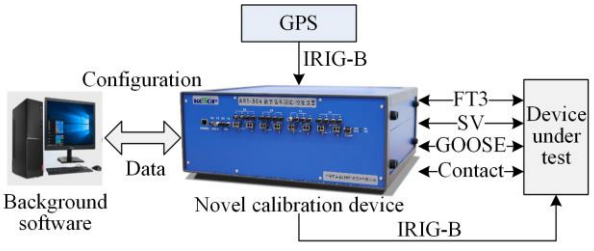


Fig. 4. Configuration and input/output display diagram of novel system.

*C. Novel Software Design*

The software of the calibration device adopts hierarchical and modular design, as shown in Fig. 5. It is mainly divided into an interaction layer, a logic layer, and a driver layer. Each layer is composed of various functional modules, which are independent of each other and use internal message interface for data interaction [19].

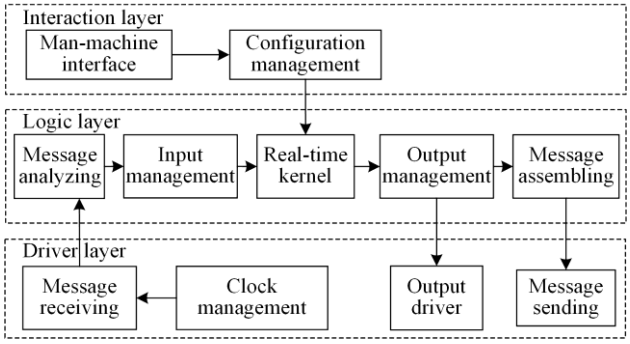


Fig. 5. Novel software design block diagram.

The interaction layer is responsible for human-computer interaction, generating configuration and controlling logical behavior.

The logic layer is responsible for extracting data, waveform fitting, logical calculation, calibration analysis and generating output data.

The driver layer is responsible for collecting data and controlling output of the driver hardware.

## IV. Key Technologies of the Novel Method

This paper presents a novel calibration method for accurate calibration for digital signals of relay protection test equipment. Since FPGA devices are superior to microcontrollers in speed and anti-interference, FPGA hardware is used to implement frequency modulation and phase locking with IRIG-B signal source and high-precision adjustment of internal clock, providing

accurate time beat for each module and achieving accurate input and output control [12], [20].

### A. Accurate Time Calibration of Input Data

High-precision internal clock management is the cornerstone for the accuracy of the novel calibration system. The frequency modulation and phase locking with the IRIG-B signal source are realized using the FPGA device, and the internal clock is adjusted with high precision to provide accurate time beat for each module [21]. The principle is illustrated in Fig. 6. When the novel system is connected to an external clock source, the clock logic calculates the difference between the internal and external clocks in real time, and the error approximation algorithm is used to accurately adjust the local clock to ensure the synchronization of internal time rhythms.

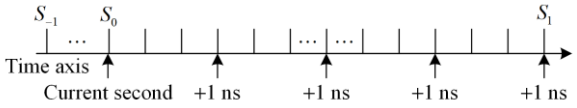


Fig. 6. Accurate time calibration of input data.

For example, if the time difference between the previous second and the local system time is 100 ns, the system adjusts the time by 100 ns in the next second. The adjustment position is calculated, e.g., the 100 MHz clock is adjusted once every 1 million clocks, i.e., 1 ns.

*1) Contact Signal Accurate Receiving*

For contact signals, the FPGA hardware performs high-frequency sampling and real-time comparison of switching input voltage. When the on-off voltage change exceeds the threshold value, time calibration is carried out immediately. After applying logic processing such as de-jitter, the initial change moment is backtracked, and is taken as the precise switching time marker.

*2) Optical Port Message Receiving*

For receiving the optical port message, the FPGA device monitors the physical layer (PHY) device of the network port, calibrates the arrival time of the leading byte of the network message, and calibrates the hardware delay of the optical port according to the parameters set by the system, so as to accurately obtain the time mark of the message arrival [22].

### B. Accurate Time Calibration of Output Data

The novel calibration system achieves accurate time output control for SV, GOOSE and contact signals, and mainly includes the following two aspects.

*1) Contact Signal Accurate Output*

Quick output node and special front hardware are used to control and reduce the uncertainty of front hardware delay. The bottom drive delay and hardware delay in the slicing time interval are compensated by the FPGA device, while the upper logic delay is compensated by the front-end system software.

*2) Optical Port Message Output*

The FPGA optimizes and implements network media access control (MAC) layer logic to directly control network PHY devices and accurately evaluate the time interval between network data preparation and actual transmission [23]. When the FPGA obtains the data packet from the bus queue, it extracts the time label, and compensates the logical delay and hardware time to obtain the time that really needs to be written into the network PHY. It then monitors the current time in real time, and accurately writes the network message at the specified time to complete the accurate time transmission.

As an example, a frame is required to be sent at 1 084 600 ns in the current second, and the sending time control logic is shown in Fig. 7. The data processing module obtains the message and time label to be sent at $t_1$. If the hardware delay takes 80 ns, to ensure that the message leaves the system at $t_3 = 1\,084\,600$ ns, it is necessary to control the message to leave the message output module at $t_2 = 1\,084\,520$ ns.

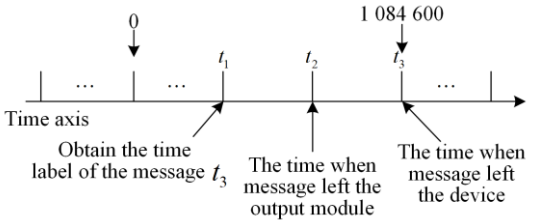


Fig. 7. Novel control logic of message sending time.

Based on accurate input and output, the action time setting can be realized, as shown in Fig. 8. The detection and calibration device records the arrival time $t_1$ of the incoming message according to the accurate time calibration method of the incoming message. At the same time, the output module obtains the output time label $t_7$ at $t_5$, and drives the output at $t_6$ according to the logic time of the output module and the output hardware delay, so as to ensure that the contact output is effective at $t_7$, while the operation time $\Delta T$ is expressed as $\Delta T = t_7 - t_1$.

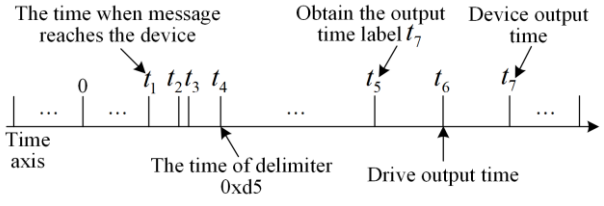


Fig. 8. Novel method of high precision action time setting.

### *C. Accurate Calibration Based on Multiple Traceability*

#### *1) Theoretical Value Traceability Based on Waveform Comparison*

When power equipment uses the sampled value signal input from the front end, the effective values can be extracted for logical judgment, analysis or resampling the sampling point. In this case, the instantaneous values at the sampling point will affect the calculation results or action behavior. Therefore, to verify the accuracy of the digital signals, it is necessary to evaluate the errors of the effective and instantaneous values.

For the amplitude and phase, NB/T 11216-2023 uses the theoretical traceability method to compare the measured digital waveform with the theoretical waveform to obtain the errors.

a) Reference Waveform Generation

According to the output setting values of the digital device under test or the digital tester (parameter information of the digital waveform intended to be output), the novel calibration device presets parameters such as sampling rate, frequency, effective value of fundamental wave and initial phase angle, and effective value of harmonic component and initial phase angle. The theoretical waveform is generated locally by matching sampling pulse according to (1), and the time scale is assigned to each sampling point as the reference waveform to calculate the errors.

$$x(t) = U_0 + \sum_{k=1}^{n} \left[ U_k \cos(k\omega t + A_k) \right] \tag{1}$$

where $U_0$ is the DC variable; $U_k$ is the harmonic amplitude; and $A_k$ is the initial phase of the $k$th harmonic.

A 4 kHz sinusoidal signal sampling rate is used as an example (sampling interval is 250 μs). The effective amplitude value of the reference waveform and the instantaneous amplitude value (including phase) of each sampling point are automatically extracted by the data processing module of the novel calibration device.

b) Automatic Waveform Alignment

In the time synchronization state, the actual output digital waveform of the device under test outputs specific initial phase angle at 0 sequence number time. Therefore, when constructing the reference waveform, the novel calibration device achieves time-domain alignment by ensuring consistency of the reference waveform 0 sequence number time and the measured waveform, thereby ensuring accurate error analysis. For certain devices under test, where the initial phase of 0 sequence time is unstable due to impaired precision or design limitation, alignment is realized by capturing a section of actual digital waveform and calculating the initial phase angle of 0 sequence time. The waveform alignment and calibration process are shown in Fig. 9, where the standard sinusoidal signal is illustrated.

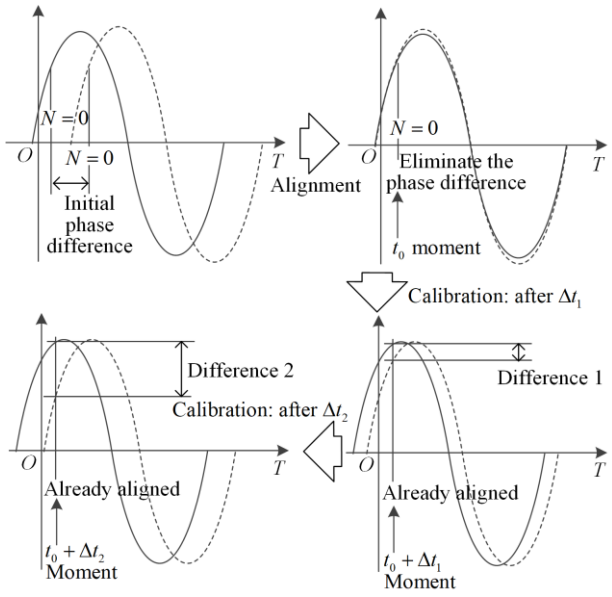


Fig. 9. Schematic diagram of waveform alignment and calibration process.

#### *2) Time Scale Value Traceability Based on Accurate Time Stamps*

An important feature of power system digital signals is the correlation with time. For digital signals with a given sampling rate, their accuracy is affected by the accuracy of rated delay and sampling interval.

Taking rated delay as an example, for a digital signal output device, it is defined as the difference between the scheduled sending time and the actual sending time, i.e., the difference between the actual sending time of No. 0 message and the reference sampling pulse time, as shown in Fig. 10.

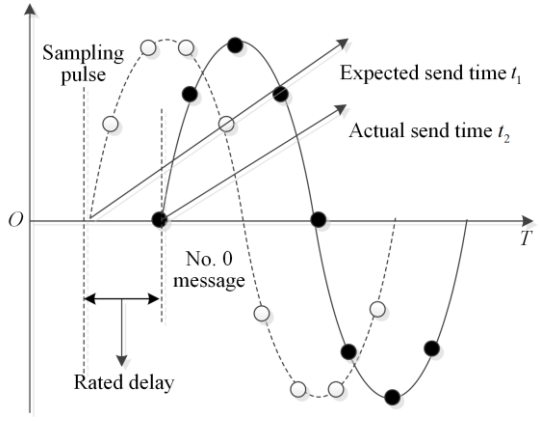


Fig. 10. Schematic diagram of digital signal rated delay.

Therefore, the detection and calibration of the rated delay can be traced upward at the time level, and the accurate time scale of each sampling point of the measured digital signal can be recorded by the testing equipment to verify the accuracy of the rated delay.

The novel calibration system features precise timestamping, implements frequency modulation and phase locking of the IRIG-B signal source within the

FPGA, supports high-precision internal clock adjustment, and provides accurate time beat for each module. For receiving optical interface packets, the FPGA monitors the PHY device of the network port, calibrates the arrival time of the leading byte of the network packet, and calibrates the hardware delay of the optical interface according to the parameters set by the system, to accurately obtain the arrival time mark of the packet. The calibration method of receiving message time is shown in Fig. 11.

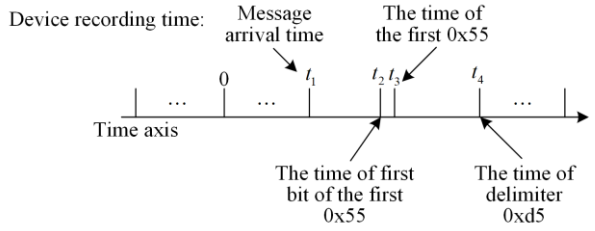


Fig. 11. Novel time calibration method for receiving messages.

As shown in Fig. 11, $t_1$ is the time when the message arrives at the device; $t_3$ is the time of the first 0x55 of the message; and $t_4$ is the moment at which the packet frame begins delimiter 0xd5. The time is traced back to the moment when $t_2$ is the first bit of the packet leader 0x55, and the hardware delay is corrected. The real time $t_1$ when the packet arrives at the device is obtained, i.e., the timestamp of the frame packet.

*3) Algorithm Traceability Based on Typical Algorithms*

In order to analyze the accuracy of the digital signals, it is necessary to extract the characteristic quantities of the measured waveform. This process relies heavily on the algorithm used, especially in cases when the frequency changes or the fundamental signals have harmonic components superimposed.

NB/T 11216-2023 specifies the typical algorithms to be used to extract parameters during digital signal calibration, and the analysis errors caused by different algorithms can be eliminated by unifying algorithms [9]. The novel calibration system implements a typical algorithm, taking three types of signals of 45 Hz/50 Hz/55 Hz as examples (same sampling rate). In the same time window, the numbers of sampling cycles of the three frequencies are different, while within a single cycle, the sampling points of the three frequencies are different. Reflected in the same coordinate system, the distribution of the three digital waveforms is shown in Fig. 12.

The novel calibration system uses fast Fourier transform (FFT) algorithm to optimize the frequency estimation, track and extract the frequency and analyze the amplitude and phase correctly [24]. For the measured digital waveform, the following steps are performed: 1) Estimate the frequency value by "zero crossing"; 2) Based on the estimated frequency, take two consecutive cycles to perform FFT. If the estimated frequency matches the actual frequency, the calculated amplitude and phase should be completely consistent across the two cycles; 3) If there is an error in the estimated frequency, the calculated amplitude and phase will drift, which is used to calculate $\Delta f$. The estimated frequency is modified for the second step of iteration, and the process continues until the error is less than the set value (0.0005 Hz, lower than the industry accuracy requirements of 0.001 Hz); 4) After correctly tracking and refining the frequency, FFT is performed again with the measured frequency to obtain the amplitude and phase [25].

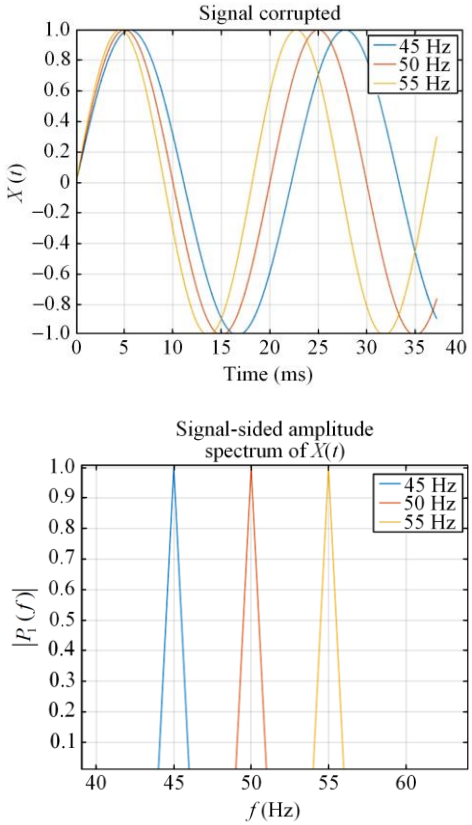


Fig. 12. Distribution of digital waveforms at different frequencies (time domain and frequency domain).

## D. Implementation of Calibration Process

*1) Amplitude and Phase Calibration*

a) Amplitude Valid Value

The novel calibration system records the measured digital signal, and the time window is no less than 1 s. The effective value of the measured digital message amplitude is set as $A$, and the novel calibration system automatically calculates the optimal value $\hat{A}$ of the amplitude estimation. The effective value error $W$ is calculated as follows:

$$W = (\hat{A} - A)/A \times 100\% \tag{2}$$

The optimal value of digital signal amplitude estimation $\hat{A}$ is calculated as follows:

$$\hat{A} = \sqrt{\sum_{n=1}^{N} A_n^2 \Big/ 2} \tag{3}$$

where $A_n$ is the amplitude of the $n$th harmonic.

b) Amplitude Instantaneous Value

For the digital signal output device, the transmission parameters need to be set, including sampling rate, amplitude, frequency, and initial phase angle. The novel calibration system records the instantaneous value $\boldsymbol{X}_n$ of all sampling points of the digital signal under test, and the time window is no less than 1 s. The initial phase angle of the digital signal is estimated according to the instantaneous value optimal estimation algorithm. The theoretical waveform is generated according to the initial phase angle and sampling interval, and the instantaneous theoretical value $\hat{\boldsymbol{X}}_n$ for all sampling points in the time window is calculated.

The calculation formula for the instantaneous value error is shown as:

$$\Delta \boldsymbol{X} = \hat{\boldsymbol{X}}_n - \boldsymbol{X}_n \tag{4}$$

$$\hat{\boldsymbol{\varepsilon}}_n = \Delta \boldsymbol{X} \big/ (\sqrt{2} \times A) \tag{5}$$

$$\hat{\boldsymbol{\varepsilon}}_{\max} = \max\left(\hat{\boldsymbol{\varepsilon}}_n\right) \tag{6}$$

where $\Delta \boldsymbol{X}$ is the instantaneous value error of the $n$th sampling point; $\hat{\boldsymbol{\varepsilon}}_n$ is the peak instantaneous error at the $n$th sampling point; and $\hat{\boldsymbol{\varepsilon}}_{\max}$ is the maximum peak instantaneous error.

For a digital AC sampling sequence of a time window $(x_1, x_2, \cdots, x_n, \cdots, x_N)$, assuming its frequency is 50 Hz, the optimal estimation algorithm for the instantaneous value is described as follows.

Kalman algorithm is used to estimate the initial phase optimal value [26]. First, the algorithm is used to estimate the initial phase $\varphi_0$ in the time window. The initial phase $\varphi_0$ and sampling parameters are then used to calculate the theoretical value $\boldsymbol{x}(t)$ of a single sampling point. The mathematical expression is as follows:

$$\boldsymbol{x}(t) = A\cos(\omega t + \varphi_0) \tag{7}$$

To filter the initial phase $\varphi_0$, a vector sequence $\begin{bmatrix} \cos\varphi_0 \\ \sin\varphi_0 \end{bmatrix}$ is used, and the mathematical representation of the signal is as follows.

$$\boldsymbol{x}(t) = \left[\alpha\cos\omega t - \alpha\sin\omega t\right]\begin{bmatrix} \cos\varphi_0 \\ \sin\varphi_0 \end{bmatrix} \tag{8}$$

where $\alpha$ is the sampling amplitude.

The corresponding Kalman equation is:

$$\begin{cases} \boldsymbol{X}_{k+1} = \boldsymbol{X}_k = \begin{bmatrix} \cos\varphi_0 \\ \sin\varphi_0 \end{bmatrix} \\ \boldsymbol{Z}_k = \left[\alpha\cos\omega t_k - \alpha\sin\omega t_k\right]\boldsymbol{X}_k + \boldsymbol{\omega}_k \end{cases} \tag{9}$$

where $\boldsymbol{Z}_k$ is the measurement value at time $k$ and $\boldsymbol{X}_k$ is the system state at time $k$.

During calibration, the frequency does not change, so the system noise variance matrix $\boldsymbol{Q} = 0$, and adaptive Kalman algorithm can be used to observe noise $\boldsymbol{R}$:

$$\boldsymbol{R} = (\boldsymbol{Z}_k - \boldsymbol{H}_k\hat{\boldsymbol{X}}_k)^{\mathrm{T}}(\boldsymbol{Z}_k - \boldsymbol{H}_k\hat{\boldsymbol{X}}_k) \tag{10}$$

where $\boldsymbol{H}_k$ is the parameters of the measurement system at time $k$ and $\hat{\boldsymbol{X}}_k$ is transposed matrix of $\boldsymbol{X}_k$.

The recursive equations are thus obtained as follows:

$$\begin{cases} \boldsymbol{X}_k = \hat{\boldsymbol{X}}_{k-1} \\ \boldsymbol{P}_k = \hat{\boldsymbol{P}}_{k-1} \\ \boldsymbol{X}_k = \boldsymbol{X}_k + \hat{\boldsymbol{K}}_k(\boldsymbol{Z}_k - \boldsymbol{H}_k\boldsymbol{X}_k) \\ \boldsymbol{K}_k = \boldsymbol{P}_k(\boldsymbol{H}_k\boldsymbol{P}_k\boldsymbol{H}_k^{\mathrm{T}} + \boldsymbol{R}_k) \\ \hat{\boldsymbol{P}}_k = (1 - \boldsymbol{K}_k\boldsymbol{H}_k)\boldsymbol{P}_k \end{cases} \tag{11}$$

where $\boldsymbol{P}_k$ represents covariance at time $k$; $\hat{\boldsymbol{P}}_{k-1}$ is transposed matrix of $\boldsymbol{P}_{k-1}$; and $\boldsymbol{K}_k$ represents Kalman Gain at time $k$.

Next, the sampling points of 10 cycles are calculated to obtain the optimal initial phase estimate:

$$\hat{\boldsymbol{X}} = \boldsymbol{X}_k = \begin{bmatrix} \cos\varphi_0 \\ \sin\varphi_0 \end{bmatrix} \tag{12}$$

The optimal estimate of the sampling point obtained from the sampling sequence is given as:

$$t_n = (n-1)\Delta t,\ n = 1, 2, \cdots, N \tag{13}$$

$$\hat{\boldsymbol{x}}_n = \left[\alpha\cos\omega t_n - \alpha\sin\omega t_n\right]\boldsymbol{X} \tag{14}$$

where $\alpha$ is the sampling amplitude; $\Delta t$ is the sampling interval; and $\boldsymbol{X}$ is the initial phase.

c) Phase Value

The device under test outputs digital messages according to the maximum number of channels, selects one of the digital channels $I$, and sets its initial phase $\varphi$. The novel calibration system analyzes the actual initial phase $\varphi'$ of the digital channel $I$. The calculation of the phase error is given as:

$$\Delta\varphi = \varphi' - \varphi \tag{15}$$

*2) Calibration of Sampling Interval and Delay*

a) Sampling Interval

The device under test sends digital messages according to the sampling rate $f_0$, and the calibration system is used to receive and count the sampling interval of 5 minutes. Sampling interval accuracy is usually expressed by sampling interval error:

$$\Delta T = T - T_0 \tag{16}$$

$$T_0 = 1/f_0 \tag{17}$$

where $T$ and $T_0$ are the measurement and reference values of the sampling interval, respectively.

Using statistical sampling interval error, the maximum error is obtained as:

$$M_{\mathrm{T}} = \max(T_i - T_0) \tag{18}$$

where $M_{\mathrm{T}}$ is the maximum sampling interval error; and $T_i$ is the actual sampling interval.

b) Rated Delay

The rated delay of the novel calibration system is $T_{\mathrm{d}}$ and a digital message is sent at the whole second $T_{\mathrm{s}}$. The moment when the novel calibration system receives the first frame of digital message with sampling serial number 0 is recorded as $T_{\mathrm{l}}$. The calculation of the rated delay measurement value $T_{\mathrm{d}}$ is given as:

$$T_{\mathrm{d}} = T_{\mathrm{l}} - T_{\mathrm{s}} \tag{19}$$

The rated delay error $\Delta T_{\mathrm{d}}$ is calculated as:

$$\Delta T_{\mathrm{d}} = T_{\mathrm{d}} - T_{\mathrm{d0}} \tag{20}$$

where $T_{\mathrm{d0}}$ is the rated delay time setting value.

*3) Calibration of Frequencies and Harmonic Wave*

a) Frequencies

The frequency of the output digital signal of the calibrated device is $f_0$, and the recording time window of the calibration system is no less than 10 s. The calibration system parses the measured digital message and obtains the best estimate of the frequency $\hat{f}$. The frequency error calculation is given as:

$$W = \frac{\hat{f} - f_0}{f_0} \times 100\% \tag{21}$$

where $W$ is the frequency error; $f_0$ is the set value; and $f$ is the measurement value.

The algorithm estimates the optimal frequency by setting frequency $f_0$ of the device under test, and this value is recorded as the estimated frequency. $\hat{f}$ is the best estimate, $\hat{f} = f_0 + \Delta f$, and $\Delta f$ is the estimated frequency difference. The input sinusoidal signal is shown as:

$$x(t) = U_{\mathrm{m}} \sin(2\pi(f_0 + \Delta f) + \alpha_0) \tag{22}$$

where $U_{\mathrm{m}}$ is the effective value of the signal; and $\alpha_0$ is the initial phase of the signal.

In the case of not knowing the real frequency, first the setting frequency $f_0$ (where $f_0 \times T_0 = 1$) is used in the Fourier transform to get the amplitude of the real frequency component $a$ and $b$:

$$a = \frac{2}{T_0}\int_0^{T_0} U_{\mathrm{m}} \sin\left(2\pi\left(f_0 + \Delta f\right)t + \alpha_0\right)\sin\left(2\pi f_0 t\right)\,\mathrm{d}t = \frac{2U_{\mathrm{m}} f_0}{\pi T_0 \Delta f (2f_0 + \Delta f)}\cos(\pi\Delta f T_0 + \alpha_0)\sin(\pi\Delta f T_0) \tag{23}$$

$$b = \frac{2}{T_0}\int_0^{T_0} U_{\mathrm{m}} \sin\left(2\pi\left(f_0 + \Delta f\right)t + \alpha_0\right)\cos\left(2\pi f_0 t\right)\,\mathrm{d}t = \frac{2U_{\mathrm{m}}(f_0 + \Delta f)}{\pi T_0 \Delta f (2f_0 + \Delta f)}\sin(\pi\Delta f T_0 + \alpha_0)\sin(\pi\Delta f T_0) \tag{24}$$

Fourier change for the second period gets the amplitude of the real frequency component $a'$ and $b'$:

$$a' = \frac{2}{T_0}\int_{T_0}^{2T_0} U_{\mathrm{m}} \sin(2\pi(f_0 + \Delta f)t + \alpha_0)\sin(2\pi f_0 t)\,\mathrm{d}t = \frac{2U_{\mathrm{m}} f_0}{\pi T_0 \Delta f (2f_0 + \Delta f)}\cos(3\pi\Delta f T_0 + \alpha_0)\sin(\pi\Delta f T_0) \tag{25}$$

$$b' = \frac{2}{T_0}\int_{T_0}^{2T_0} U_{\mathrm{m}} \sin(2\pi(f_0 + \Delta f)t + \alpha_0)\cos(2\pi f_0 t)\,\mathrm{d}t = \frac{2U_{\mathrm{m}}(f_0 + \Delta f)}{\pi T_0 \Delta f (2f_0 + \Delta f)}\sin(3\pi\Delta f T_0 + \alpha_0)\sin(\pi\Delta f T_0) \tag{26}$$

Equations (23), (24), and (25), (26) are respectively used to define *A* and *B* as:

$$A = \frac{a}{a'} = \frac{\cos(\pi\Delta f T_0 + \alpha_0)}{\cos(3\pi\Delta f T + \alpha_0)} \tag{27}$$

$$B = \frac{b}{b'} = \frac{\sin(\pi\Delta f T_0 + \alpha_0)}{\sin(3\pi\Delta f T_0 + \alpha_0)} \tag{28}$$

Equations (27) and (28) are further expanded to obtain:

$$A = \frac{1}{\cos(2\pi\Delta f T_0) - \sin(2\pi\Delta f T_0)\dfrac{\sin(\pi\Delta f T_0 + \alpha_0)}{\cos(\pi\Delta f T_0 + \alpha_0)}} \tag{29}$$

$$B = \frac{1}{\cos(2\pi\Delta f T_0) + \sin(2\pi\Delta f T_0)\dfrac{\cos(\pi\Delta f T_0 + \alpha_0)}{\sin(\pi\Delta f T_0 + \alpha_0)}} \tag{30}$$

Equations (29) and (30) are simplified as:

$$\cos(2\pi\Delta f T_0) = \frac{AB + 1}{A + B} = \frac{ab + a'b'}{ab' + a'b} \tag{31}$$

Thus, the estimated frequency difference $|\Delta f|$ and the real frequency $\hat{f}$ are obtained by using (32) and (33), respectively:

$$|\Delta f| = \frac{1}{2\pi T_0}\arccos\left(\frac{ab + a'b'}{ab' + a'b}\right) \tag{32}$$

$$\hat{f} = f_0 + |\Delta f| \tag{33}$$

b) Harmonics Wave

The calibration system records the digital message with a time window of no less than 10 s, and performs harmonic decomposition of the digital message according to the algorithm. The amplitude of each harmonic wave is mathematically expressed as:

$$\hat{A}_0, \hat{A}_1, \cdots, \hat{A}_i \tag{34}$$

where $\hat{A}_0$ is the amplitude of the DC component and $\hat{A}_i$ is the amplitude of the $i$th harmonic wave, with $i=1$ representing the fundamental component.

The harmonic amplitude error is calculated as follows:

$$\hat{W}_n = (\hat{A}_n - A_{n0})/A_{n0} \times 100\% \tag{35}$$

where $W_n$ is the $n$th harmonic error and $A_{n0}$ is the harmonic amplitude.

The harmonic decomposition adopts the windowed FFT algorithm. The Blackman-Harris window function with high computational accuracy is selected, and its number time domain expression is:

$$W(n) = 0.35875 - 0.48829\cos\frac{2\pi n}{N-1} + 0.14128\cos\frac{4\pi n}{N-1} - 0.01169\cos\frac{6\pi n}{N-1} \tag{36}$$

In a single frequency signal $x(t)$, the frequency is $f_0$, the amplitude is $A$, and the initial phase is $\phi$. After resampling with sampling frequency $f_s (f_s \geqslant 2f_0)$, the expression is as follows:

$$x(n) = A\sin\left(2\pi\frac{f_0}{f_s}\times n + \phi\right) \tag{37}$$

After adding window $W(n)$, the Fourier transform of the signal is as follows:

$$X(f) = \sum_{n=1}^{\infty}(x(n)\times W(n)\times e^{j2\pi fn}) = 0.5j\left\{e^{j\phi}W\left[\frac{2\pi(f-f_0)}{f_s}\right] - e^{j\phi}W\left[\frac{2\pi(f+f_0)}{f_s}\right]\right\} \tag{38}$$

The continuous spectrum expression near $f_0$ is:

$$X(f) = (A/2j)\times e^{j\phi}W\left[\frac{2\pi(f-f_0)}{f_s}\right] \tag{39}$$

Discrete sampling is carried out, and the discrete Fourier transform expression is as follows:

$$X(f) = (A/2j)e^{j\phi}W\left[\frac{2\pi(n\Delta f - f_0)}{f_s}\right] \tag{40}$$

where $\Delta f = 1/NT$, with $N$ indicating the truncation length of the data. The peak value appears at $f_0 = k_0\Delta f$, and $k_0$ is generally not an integer. Let the spectral lines on the left and right sides of $k_0$ be $k_1$ and $k_2$ spectral lines, respectively, which means that the two spectral lines taken should be the spectral lines with the largest and sub-large values near the peak point. $k_1 \leqslant k_0 \leqslant k_2$ $(k_2 = k_1 + 1)$, and the two spectral lines have magnitudes of $y_1 = |X(k_1\Delta f)|$, $y_2 = |X(k_2\Delta f)|$. Since $0 \leqslant k_0 - k_1 \leqslant 1$, the auxiliary parameter $a = k_0 - k_2 - 0.5$, $a \in [-0.5, 0.5]$, and there is:

$$\frac{y_2 - y_1}{y_2 + y_1} = \frac{\left|W\left[\frac{2\pi(-a+0.5)}{N}\right]\right| - \left|W\left[\frac{2\pi(-a-0.5)}{N}\right]\right|}{\left|W\left[\frac{2\pi(-a+0.5)}{N}\right]\right| + \left|W\left[\frac{2\pi(-a-0.5)}{N}\right]\right|} \tag{41}$$

Set $b = (y_2 - y_1)/(y_2 + y_1)$, then (41) is a function with $a$ as the independent variable and $b$ as the dependent variable. $b = f(a)$, and its inverse function is $a = f^{-1}(b)$. Using polynomial approximation method [27], $a$ can be calculated:

$$a = 2.6197085b + 0.2865675b^3 + 0.1283b^5 + 0.08024b^7 \tag{42}$$

The amplitude expression modified by the Blackman-Harris window is [28]:

$$A = \frac{(y_1 + y_2)\left(\begin{matrix}3.06539676 + 0.965559979a^2 + \\ 0.163556a^4 + 0.01985a^6\end{matrix}\right)}{N} \tag{43}$$

The amplitudes of fundamental wave and each harmonic are calculated using the above method.

## V. Performance Analysis

In this paper, a special accuracy verification system is set up to test the input and output accuracy of the novel calibration system, as shown in Fig. 13. When the novel calibration system and the relay protection test equipment perform closed-loop testing, to achieve the accuracy verification of the input and output signals, the contact signals are connected to the oscilloscope and the digital signals (SV, FT3 or GOOSE) are connected to the network recorder for monitoring.

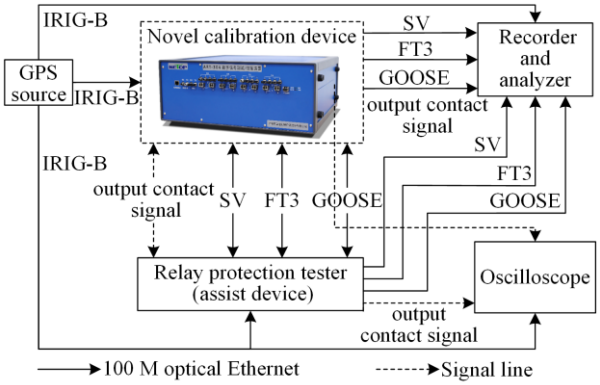


Fig. 13. Diagram of the novel calibration system's accuracy verification structure.

### *A. Time Scale Accuracy Verification of Input and Output Signals*

Since the time measurement of the relay protection test equipment requires an accuracy of 100 μs, the novel calibration system is fully capable of meeting calibration needs if it achieves an accuracy of 10 μs [2].

The accuracy verification method of input signals is as follows. The relay protection test equipment sends

periodically SV, GOOSE or contact signal, while the novel calibration system records the signal arrival time as $T_1$, the recorder or oscilloscope records the signal arrival time as $T_2$, so $T_1 - T_2$ is the error of the input signals.

The accuracy verification method of output signals is as follows. The novel calibration system sends SV, GOOSE or contact signal at $T_1$, and the recorder or oscilloscope records the arrival time of the signals at $T_2$, so $T_1 - T_2$ is the error of the output signals.

Each type of signal is tested 1000 times, and the statistics and analysis results are shown in Table I and Fig. 14. The mean value, maximum value, minimum value, and standard deviation are calculated. According to the test results, even the maximum error can still meet the calibration requirements (better than 10 μs). Compared with the test results of existing calibration systems, both calibration accuracy and stability have been significantly improved.

The mean error values in Table I are the mean values of 1000 trials, and the standard deviations represent the variability of the error across the 1000 trials. The test data show that the precision of digital signal acquisition and output time scale is better than ± 100 ns, and that of contact signal acquisition and output time scale is better than ± 10 μs, which meets the application requirement of ± 10 μs.

TABLE I
DATA ANALYSIS FOR ACCURACY OF INPUT AND OUTPUT SIGNALS

| Input/output | Signal type | Recommended values (μs) | Errors | | | |
|---|---|---|---|---|---|---|
| | | | Minimum | Mean | Maximum | Standard deviation |
| Input | SV | 10 | 28 ns | 51.67 ns | 79 ns | 10.79 ns |
| | GOOSE | 10 | 31 ns | 52.71 ns | 77 ns | 10.88 ns |
| | Contact signals | 10 | 1.701 μs | 2.606 μs | 3.729 μs | 0.499 μs |
| Output | SV | 10 | 29 ns | 52.37 ns | 76 ns | 10.76 ns |
| | GOOSE | 10 | 30 ns | 52.29 ns | 78 ns | 10.69 ns |
| | Contact signals | 10 | 0.782 μs | 1.310 μs | 1.876 μs | 0.238 μs |

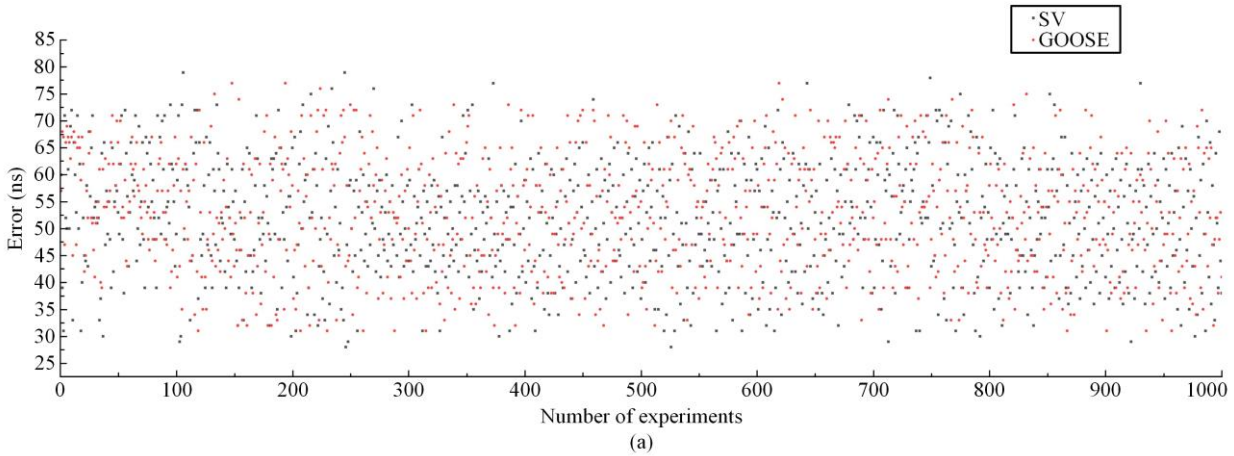

(a)

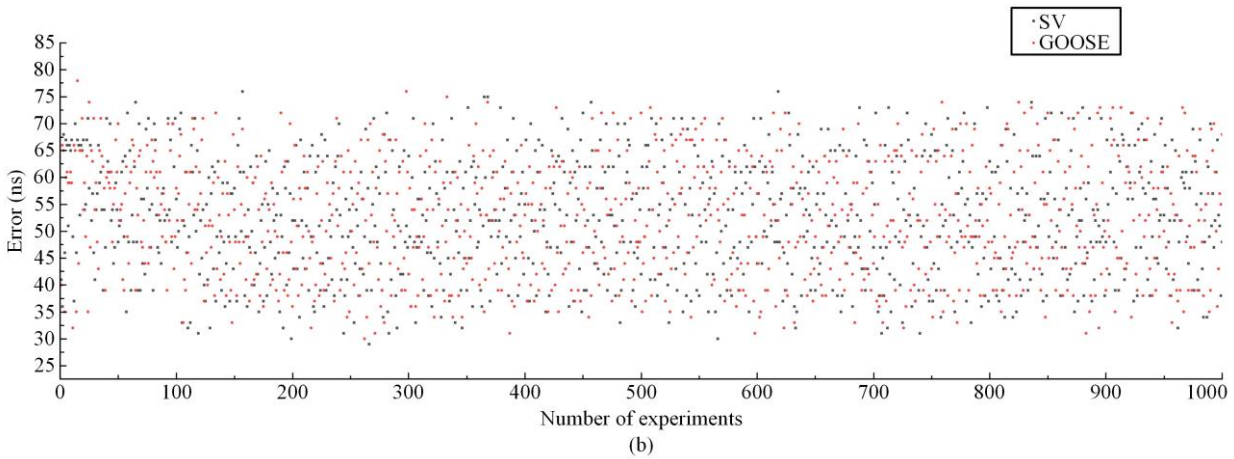

(b)

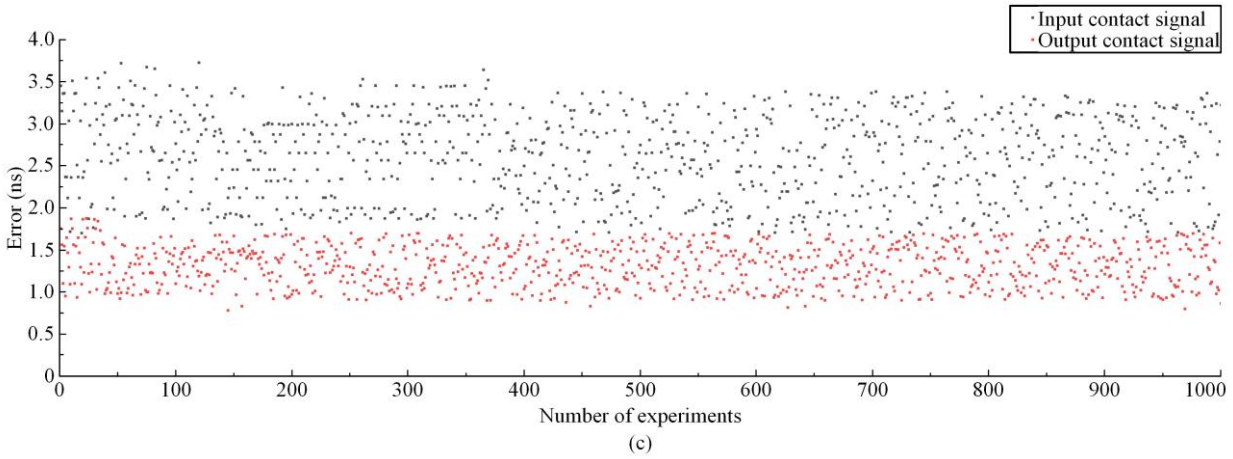


Fig. 14. Time accuracy of input/output signals based on experimental data. (a) Input digital signals (SV/GOOSE). (b) Output digital signals (SV/GOOSE). (c) Contact signals.

### *B. Digital Signal Parameters Engineering Application Verification*

The novel method presented in this paper has been applied to the test and calibration of relay protection test equipment. It has carried out calibration work for thousands of products by many manufacturers, providing accurate and rapid calibration results. The calibration results of 1000 relay protection test equipment are presented here, including 400 digital test equipment, 400 handheld optical digital test equipment, and 200 digital-analog integrated test equipment for relay protection. The results are shown in Table II. Please note that: 1) The measured instantaneous amplitude values in the table refer to the instantaneous peak values of the waves; and 2) The harmonic measurement results refer to the output values under 20% superimposed 13th harmonic condition.

TABLE II
DATA ANALYSIS FOR CALIBRATION RESULTS OF 1000 RELAY PROTECTION TEST EQUIPMENT

| Accuracy parameter | Output setting value | Absolute value of errors | | | | Pass rate (%) |
|---|---|---|---|---|---|---|
| | | Minimum | Mean | Maximum | Standard deviation | |
| Current amplitude valid value (A) | 5.000 00 | 0.000 08 | 0.000 49 | 0.000 99 | 0.000 27 | 100.0 |
| Voltage amplitude valid value (V) | 10.000 00 | 0.000 60 | 0.002 39 | 0.004 69 | 0.000 81 | 100.0 |
| Current amplitude instantaneous value (A) | 100.000 00 | 0.000 15 | 0.000 64 | 0.003 99 | 0.000 63 | 100.0 |
| Voltage amplitude instantaneous value (V) | 500.000 00 | 0.000 42 | 0.001 78 | 0.004 74 | 0.000 65 | 100.0 |
| Phase (°) | 30.000 00 | 0.000 40 | 0.001 28 | 0.002 18 | 0.000 43 | 100.0 |
| Rated delay (μs) | 500.000 | 0.000 20 | 0.051 42 | 0.197 76 | 0.039 21 | 100.0 |
| Sampling interval (μs) | 250.000 | 0.000 06 | 0.026 92 | 0.121 72 | 0.028 55 | 100.0 |
| Frequency (Hz) | 10.000 0 | 0.000 00 | 0.000 42 | 0.000 90 | 0.000 24 | 100.0 |
| 13th harmonics (%) | 20.000 | 0.000 | 0.033 | 0.089 | 0.022 | 100.0 |

In order to verify the test and calibration ability for abnormal digital signals, real time digital simulator (RTDS) is used to simulate the digital waveform of the SV message under test to generate abnormal errors, and 10 000 tests are performed [29]. Abnormal SV digital signal types include: abnormal current sampling value jump; voltage sampling value frame lost; double A/D inconsistency; out of time synchronization; ineffective quality; abnormal large numbers; and output packet jitter. The results are shown in Table III. Through 10 000 sets of simulation data, it is proved that the false alarm rate is less than 0.01%.

TABLE III
ABNORMAL SV DIGITAL SIGNAL SIMULATION

| No. | Type of abnormal SV signal | Number of tests | Number of passes | Pass rate (%) |
|---|---|---|---|---|
| 1 | Abnormal current sampling value jump | 10 000 | 0 | 0.00 |
| 2 | Voltage sampling value frame lost | 10 000 | 0 | 0.00 |
| 3 | Double A/D inconsistency | 10 000 | 0 | 0.00 |
| 4 | Out of time synchronization | 10 000 | 0 | 0.00 |
| 5 | Ineffective quality | 10 000 | 0 | 0.00 |
| 6 | Abnormal large numbers | 10 000 | 0 | 0.00 |
| 7 | The output packet jitter | 10 000 | 0 | 0.00 |

### C. Multi-signal Mode Accuracy Verification

The novel method has also been applied to the test and calibration of complex operations of relay protection test equipment, such as time measurement, time control and so on. This paper presents the test results of 200 equipment with time measurement and time control functions, including 80 digital test equipment, 80 handheld optical digital test equipment, and 40 digital-analog integrated test equipment for relay protection.

The action time accuracy of the novel calibration method can meet the requirements of testing time measurement operation. According to the type of action time specified in the standard, six types of action time setting accuracy (calibration accuracy should be better than 10 μs) are verified in this paper. The relay protection test equipment periodically sends digital signal 1, and the network recorder device (or oscilloscope) records the arrival time of digital signal as $T_1$. After receiving the digital signal, the novel calibration system delays $T_0$ to output the digital signal 2, and the network recorder device (or oscilloscope) records the arrival time of the digital signal as $T_2$. $T_2 - T_1$ is the actual operation time $\Delta T$, and $\Delta T - T_0$ is the accuracy error of the action time. A total of 200 tests are carried out, the results are shown in Tables IV–IX.

TABLE IV
ACCURACY OF ACTION TIME (FROM RECEIVING SV TO SENDING GOOSE)

| $T_0$ (ms) | Errors (ms) | | | |
|---|---|---|---|---|
| | Minimum | Mean | Maximum | Standard deviation |
| 1 | 0.000 028 | 0.000 114 | 0.000 162 | 0.000 032 |
| 50 | 0.000 033 | 0.000 123 | 0.000 195 | 0.000 028 |
| 100 | 0.000 046 | 0.000 126 | 0.000 197 | 0.000 026 |
| 1000 | 0.000 063 | 0.000 133 | 0.000 214 | 0.000 024 |
| 10 000 | 0.000 088 | 0.000 135 | 0.000 228 | 0.000 021 |
| 99 999 | 0.000 113 | 0.000 149 | 0.000 249 | 0.000 023 |

TABLE V
ACCURACY OF ACTION TIME (FROM RECEIVING SV TO SENDING CONTACT SIGNAL)

| $T_0$ (ms) | Errors (ms) | | | |
|---|---|---|---|---|
| | Minimum | Mean | Maximum | Standard deviation |
| 1 | 0.001 027 | 0.001 719 | 0.002 901 | 0.000 436 |
| 50 | 0.001 382 | 0.002 350 | 0.003 020 | 0.000 372 |
| 100 | 0.001 259 | 0.002 429 | 0.003 141 | 0.000 304 |
| 1000 | 0.001 436 | 0.002 342 | 0.003 021 | 0.000 349 |
| 10 000 | 0.001 826 | 0.002 540 | 0.003 250 | 0.000 306 |
| 99 999 | 0.001 923 | 0.00 2851 | 0.003 565 | 0.000 403 |

TABLE VI
ACCURACY OF ACTION TIME (FROM RECEIVING GOOSE TO SENDING GOOSE)

| $T_0$ (ms) | Errors (ms) | | | |
|---|---|---|---|---|
| | Minimum | Mean | Maximum | Standard deviation |
| 1 | 0.000 029 | 0.000 085 | 0.000 176 | 0.000 030 |
| 50 | 0.000 029 | 0.000 082 | 0.000 187 | 0.000 033 |
| 100 | 0.000 032 | 0.000 128 | 0.000 202 | 0.000 044 |
| 1000 | 0.000 043 | 0.000 159 | 0.000 219 | 0.000 036 |
| 10 000 | 0.000 061 | 0.000 172 | 0.000 320 | 0.000 059 |
| 99 999 | 0.000 083 | 0.000 191 | 0.000 436 | 0.000 093 |

TABLE VII
ACCURACY OF ACTION TIME (FROM RECEIVING GOOSE TO SENDING CONTACT SIGNAL)

| $T_0$ (ms) | Errors (ms) | | | |
|---|---|---|---|---|
| | Minimum | Mean | Maximum | Standard deviation |
| 1 | 0.000 906 | 0.001 581 | 0.002 933 | 0.000 469 |
| 50 | 0.001 317 | 0.002 300 | 0.003 415 | 0.000 406 |
| 100 | 0.001 243 | 0.002 421 | 0.003 487 | 0.000 345 |
| 1000 | 0.001 451 | 0.002 346 | 0.003 322 | 0.000 348 |
| 10 000 | 0.001 798 | 0.002 541 | 0.003 423 | 0.000 309 |
| 99 999 | 0.001 941 | 0.002 830 | 0.003 598 | 0.000 406 |

TABLE VIII
ACCURACY OF ACTION TIME (FROM RECEIVING CONTACT SIGNAL TO SENDING GOOSE)

| $T_0$ (ms) | Errors (ms) | | | |
|---|---|---|---|---|
| | Minimum | Mean | Maximum | Standard deviation |
| 1 | 0.001 901 | 0.002 475 | 0.003 789 | 0.000 518 |
| 50 | 0.002 310 | 0.003 194 | 0.003 832 | 0.000 357 |
| 100 | 0.002 682 | 0.003 191 | 0.003 769 | 0.000 298 |
| 1000 | 0.002 856 | 0.003 300 | 0.003 983 | 0.000 194 |
| 10 000 | 0.003 101 | 0.003 243 | 0.004 102 | 0.000 218 |
| 99 999 | 0.003 104 | 0.003 817 | 0.004 199 | 0.000 290 |

TABLE IX
ACCURACY OF ACTION TIME (FROM RECEIVING CONTACT SIGNAL TO SENDING CONTACT SIGNAL)

| $T_0$ (ms) | Errors (ms) | | | |
|---|---|---|---|---|
| | Minimum | Mean | Maximum | Standard deviation |
| 1 | 0.003 107 | 0.003 638 | 0.004 384 | 0.000 299 |
| 50 | 0.003 719 | 0.004 566 | 0.005 385 | 0.000 404 |
| 100 | 0.003 988 | 0.004 703 | 0.005 383 | 0.000 312 |
| 1000 | 0.003 965 | 0.004 809 | 0.005 398 | 0.000 330 |
| 10 000 | 0.004 424 | 0.005 189 | 0.005 892 | 0.000 303 |
| 99 999 | 0.004 881 | 0.005 451 | 0.006 097 | 0.000 301 |

The mean value of the difference in Tables IV–IX is the mean value of the 200 trials, and the standard deviation is the standard deviation of the samples. The test data shows that the action time accuracy of the novel calibration system for all types of signals meets the index of ±10 μs, thus qualifying the conclusion.

The time measurement accuracy of the novel calibration system can meet the requirements of testing action time. According to the type of action time specified in the standard, six kinds of action time setting accuracy (calibration accuracy should be better than 10 μs) are verified in this paper. The novel calibration system sends digital signal 1 to relay protection test equipment and the network recorder device (or oscilloscope) at $T_1$, and the network recorder device (or oscilloscope) records the arrival time of digital signal as $T_1'$. The relay protection test equipment outputs a digital signal 2 to the novel calibration system and the network recorder device (or oscilloscope) after delaying $T_0$, and the novel calibration device records the arrival time of the digital signal 2 as $T_2$. The network recorder device (or oscilloscope) records the arrival time of the digital signal 2 as $T_2'$. $\Delta T = T_2 - T_1$ is the time measurement obtained by the novel calibration system, $\Delta T' = T_2' - T_1'$ is the actual time measurement, and $\Delta T' - \Delta T$ is the accuracy error of the time measurement. A total of 200 tests are carried out, and the results are shown in Tables X–XV.

According to Tables X–XV, the mean absolute value of the novel system is 2.165 μs, compared to 30.423 μs for other existing systems, representing a significant accuracy improvement of 92.88%. Since SV and GOOSE are already digitized signals, and the acquisition of contact signals needs to be converted into 1/0 digital signals after digitization, there is a significant difference in the accuracy of contact signals and SV/GOOSE. Therefore, for time measurement accuracy that only contains SV/GOOSE signals, the requirement of 100 μs does meet the practical industry requirements for the 10 μs SV/GOOSE time scale accuracy. Thus, it is recommended to modify DL/T 1501-2016, DL/T 1944-2018, DL/T 2646-2023, as shown in Table XVI.

TABLE X
ACCURACY OF TIME MEASUREMENT (FROM SENDING SV TO RECEIVING GOOSE)

| $T_0$ (ms) | Errors (ms) | | | |
|---|---|---|---|---|
| | Minimum | Mean | Maximum | Standard deviation |
| 1 | 0.000 024 | 0.000 105 | 0.000 163 | 0.000 037 |
| 50 | 0.000 031 | 0.000 112 | 0.000 198 | 0.000 036 |
| 100 | 0.000 036 | 0.000 120 | 0.000 191 | 0.000 031 |
| 1000 | 0.000 063 | 0.000 129 | 0.000 221 | 0.000 027 |
| 10 000 | 0.000 092 | 0.000 135 | 0.000 231 | 0.000 021 |
| 99 999 | 0.000 112 | 0.000 150 | 0.000 251 | 0.000 025 |

TABLE XI
ACCURACY OF TIME MEASUREMENT (FROM SENDING SV TO RECEIVING CONTACT SIGNAL)

| $T_0$ (ms) | Errors (ms) | | | |
|---|---|---|---|---|
| | Minimum | Mean | Maximum | Standard deviation |
| 1 | 0.001 021 | 0.001 736 | 0.002 889 | 0.000 447 |
| 50 | 0.001 319 | 0.002 342 | 0.002 957 | 0.000 370 |
| 100 | 0.001 322 | 0.002 422 | 0.003 113 | 0.000 301 |
| 1000 | 0.001 337 | 0.002 320 | 0.003 021 | 0.000 364 |
| 10 000 | 0.001 811 | 0.002 469 | 0.003 185 | 0.000 336 |
| 99 999 | 0.001 902 | 0.002 794 | 0.003 527 | 0.000 408 |

TABLE XII
ACCURACY OF TIME MEASUREMENT (FROM SENDING GOOSE TO RECEIVING GOOSE)

| $T_0$ (ms) | Errors (ms) | | | |
|---|---|---|---|---|
| | Minimum | Mean | Maximum | Standard deviation |
| 1 | 0.000 028 | 0.000 086 | 0.000 166 | 0.000 029 |
| 50 | 0.000 027 | 0.000 081 | 0.000 175 | 0.000 031 |
| 100 | 0.000 031 | 0.000 127 | 0.000 198 | 0.000 043 |
| 1000 | 0.000 039 | 0.000 157 | 0.000 214 | 0.000 036 |
| 10 000 | 0.000 054 | 0.000 165 | 0.000 312 | 0.000 055 |
| 99 999 | 0.000 076 | 0.00 0180 | 0.000 424 | 0.000 075 |

TABLE XIII
ACCURACY OF TIME MEASUREMENT (FROM SENDING GOOSE TO RECEIVING CONTACT SIGNAL)

| $T_0$ (ms) | Errors (ms) | | | |
|---|---|---|---|---|
| | Minimum | Mean | Maximum | Standard deviation |
| 1 | 0.001 027 | 0.002 576 | 0.003 964 | 0.000 842 |
| 50 | 0.001 923 | 0.002 850 | 0.003 998 | 0.000 537 |
| 100 | 0.002 024 | 0.003 479 | 0.004 104 | 0.000 413 |
| 1000 | 0.002 960 | 0.003 776 | 0.004 486 | 0.000 300 |
| 10 000 | 0.003 021 | 0.003 964 | 0.004 676 | 0.000 320 |
| 99 999 | 0.003 159 | 0.004 270 | 0.004 899 | 0.000 340 |

TABLE XIV
ACCURACY OF TIME MEASUREMENT (FROM SENDING CONTACT SIGNAL TO RECEIVING GOOSE)

| $T_0$ (ms) | Errors (ms) | | | |
|---|---|---|---|---|
| | Minimum | Mean | Maximum | Standard deviation |
| 1 | 0.000 827 | 0.001 510 | 0.002 159 | 0.000 313 |
| 50 | 0.001 208 | 0.001 854 | 0.002 629 | 0.000 331 |
| 100 | 0.001 313 | 0.001 971 | 0.002 643 | 0.000 309 |
| 1000 | 0.001 521 | 0.002 059 | 0.003 161 | 0.000 307 |
| 10 000 | 0.001 702 | 0.002 222 | 0.003 097 | 0.000 295 |
| 99 999 | 0.001 898 | 0.002 400 | 0.003 898 | 0.000 316 |

TABLE XV
ACCURACY OF TIME MEASUREMENT (FROM SENDING CONTACT SIGNAL TO RECEIVING CONTACT SIGNAL)

| $T_0$ (ms) | Errors (ms) | | | |
|---|---|---|---|---|
| | Minimum | Mean | Maximum | Standard deviation |
| 1 | 0.003 812 | 0.004 668 | 0.005 260 | 0.000 348 |
| 50 | 0.003 854 | 0.004 713 | 0.005 892 | 0.000 510 |
| 100 | 0.004 104 | 0.004 781 | 0.005 893 | 0.000 363 |
| 1000 | 0.003 969 | 0.004 989 | 0.005 926 | 0.000 419 |
| 10 000 | 0.004 229 | 0.005 245 | 0.005 975 | 0.000 346 |
| 99 999 | 0.004 533 | 0.005 503 | 0.006 419 | 0.000 348 |

TABLE XVI
SIX TYPES OF TIME MEASUREMENT (TIME CONTROL)

| No. | Types | Accuracy | Range (ms) |
|---|---|---|---|
| 1 | From sending SV to receiving GOOSE | ±10 μs (1 ms < $t$ ≤ 100 ms) | 1–99 999 |
| 2 | From sending GOOSE to receiving GOOSE | ±0.01% (100 ms < $t$ ≤ 99 999 ms) | |
| 3 | From sending SV to receiving input contact signal | ± 100 μs (1 ms < $t$ ≤ 100 ms); | |
| 4 | From sending GOOSE to receiving input contact signal | | |
| 5 | From sending output contact signal to receiving GOOSE | ±0.1 % (100 ms < $t$ ≤ 99 999 ms) | |
| 6 | From sending output contact signal to receiving input contact signal | | |

### *D. Anti-interference Verification*

In addition to laboratory testing, the novel calibration method has also been applied to industrial production environment, and its anti-interference capability is verified by referring to the electromagnetic compatibility requirements of standards IEC 60255-22-3: 2007, IEC 60255-22-4: 2008, IEC 60255-22-1:2007, IEC 60255-25: 2000, and DL/T 1501-2016 [30].

Engineering application proves that the novel calibration method operates satisfactory, can receive and analyze the error of each parameter of the digital signal outputs from different types of relay protection test equipment correctly, and the measurement results meet the requirements. Moreover, the statistical data of the last two years of calibration tests show that, compared with traditional test methods, the calibration equipment proposed in this paper significantly improves the test efficiency, and the calibration cycle is reduced by 85.7 %.

## VI. CONCLUSION

The novel calibration method presented in this paper improves the accuracy and efficiency of digital signal calibration of relay protection test equipment and promotes standardization. Based on FPGA, accurate input and output control is achieved, and the full index accuracy calibration of digital signals for relay protection test equipment is achieved from three aspects: theoretical value traceability, time scale value traceability and algorithm traceability. The novel calibration method has helped to form the industry standard NB/T 11216-2023, and has calibrated more than 1000 relay protection test equipment within one year after the standard was published. The following conclusion and recommendation are drawn from the experiment data:

1) The time scale accuracy of the input and output digital signals of the novel calibration device is higher than ±10 μs, and digital signal parameter calibration, time measurement, time control calibration accuracy and anti-interference ability all meet the related standard requirements;

2) It is recommended to optimize the industry standard DL/T 1501-2016, DL/T 1944-2018 and DL/T 2646-2023. The requirements for the time measurement and time control indicators of SV/GOOSE and contact signals should be differentiated according to different signal types.

Given the absence of an established international standard for relay protection test equipment, the research presented in this paper holds significant reference value for future efforts toward international standardization.

## ACKNOWLEDGMENT

Not applicable.

## AUTHORS' CONTRIBUTIONS

Yan Huang: full-text writing, designing the study, and experiment. Hadi Nabipour Afrouzi: revising the first draft, construction of the paper framework, and reviewing. Hieng Tiong Su: supervision, reviewing, and improving the manuscript. Yuan Ping: supervision and reviewing. Ismat Hijazin: reviewing and improving the manuscript. Yangtao Xu: software, experiment, and reviewing. Ke Yan: software and experiment. All authors read and approved the final manuscript.

## FUNDING

This work is supported by the Key Technologies R&D Program of Henan Province (No. 242102211065) and Postgraduate Education Reform and Quality Improvement Project of Henan Province (No. YJS2025GZZ36).

## AVAILABILITY OF DATA AND MATERIALS

Not applicable.

## DECLARATIONS

Competing interests: The authors declare that they have no known competing financial interests or personal relationships that could have appeared to influence the work reported in this article.

## AUTHORS' INFORMATION

**Yan Huang** received the B.Eng. degree in telecommunication engineering and management from the Beijing University of Posts and Telecommunications, Beijing, China, in 2016. He is pursuing a Ph.D. degree in Faculty of Engineering, Computing and Science, Swinburne

University of Technology Sarawak Campus, Kuching, Sarawak, Malaysia. His research interests include intelligent substation automation equipment and system, digital signal test and calibration technology, power system information security test technology.

**Hadi Nabipour Afrouzi** had received his M.E and Ph.D. degree in electrical engineering from Universiti Teknologi Malaysia, Johor, Malaysia, in 2011, and in 2015, respectively. Currently he is working as a senior lecturer in Birmingham City University, UK. His research interests are renewable energy, life cycle assessment, environmental impacts, sizing and optimization of hybrid system, modeling of fault in high voltage insulators. His expertise in the field of renewable energy and high voltage insulators has earned him an editorial board member of Journals, general chair of international conference and reviewer in national and international conference and journals. He is a chartered engineer from engineers Australia.

**Hieng Tiong Su** received his B.Eng. degree in electrical engineering and electronics from the University of Liverpool, UK, in 1994, and a Ph.D. degree in electronic and electrical engineering from the University of Birmingham, UK, in 2001. From 1994 to 1997, he was a communication engineer with Telecom Malaysia. After completing his PhD, he worked as a research fellow in the Department of Electronic, Electrical, and Computer Engineering, University of Birmingham, UK. From 2006, he has been with the Swinburne University of Technology Sarawak Campus. Currently, he is the professor and dean of the Faculty of Engineering, Computing and Science. His research interests include RF and microwave engineering covering RF energy harvesting, design of RF and microwave passive devices such as novel compact multimode resonators and filters for both narrowband and wideband applications, dual-band filters and substrate integrated waveguide.

**Yuan Ping** received the Ph.D. degree in information security from the Beijing University of Posts and Telecommunications in 2012. He is a professor with the School of Information Engineering, Xuchang University. His research interests include machine learning, AI Security, public key cryptography, data privacy and security, and cloud and edge computing.

**Ismat Hijazin** received his undergraduate and postgraduate degrees in electrical engineering from Bradley University, Peoria Illinois, USA. Currently he serves as a senior lecturer at Swinburne University of Technology, Melbourne Australia and a member of Engineers Australia Accreditation Panel. His research interests include FPGA systems based designs, real time hardware implementation of DSP algorithms, machine vision, and RF electronic design.

**Yangtao Xu** received the B.Eng. degree in measurement and control technology and instrument from Tianjin University of Technology, China, in 2013, and the M.Eng. degree in control engineering from Southwest Petroleum University, China, in 2016. He is currently the engineer in Xuchang KETOP Testing Research Institute Co.,Ltd., China. His research interests include the electromagnetic compatibility testing technology for power system relay protection and automation products, fault diagnosis of electrical equipment.

**Ke Yan** received the M.Eng. degree in Xi'an University of Science and Technology, Xi'an, China, in 2023. He is currently the senior engineer in Xuchang KETOP Testing Research Institute Co.,Ltd., China. His research interests include the function and performance test technology of power system relay protection and automation products, communication protocol testing technology of power equipment.

## REFERENCES

[1] V. Leitloff, H. Chen, and D. Chen *et al.*, "Towards a standardisation for digital inputs and outputs of protection functions in IEC 60255 series," *Protection and Control of Modern Power Systems*, vol. 7, no. 2, pp. 1-11, Apr. 2022.

[2] A. Hassan, H. N. Afrouzi, and C. H. Siang *et al.*, "A survey and bibliometric analysis of different communication technologies available for smart meters," *Cleaner Engineering and Technology*, vol. 7, Apr. 2022.

[3] Z. Yao, P. Wang, and G. Chen *et al.*, "Development and performance analysis of a measurement error test and calibration device for a merging unit tester in a power system," *Power System Protection and Control*, vol. 50, no. 2, pp. 119-126, Jan. 2022. (in Chinese)

[4] Y. Huang, H. N. Afrouzi, and C. L. Wooi *et al.*, "Design and performance evaluation of a novel time measurement calibration device for electric power systems," *Iranian Journal of Electrical and Electronic Engineering*, vol. 21, no. 2, pp. 1-10, Apr. 2025.

[5] Measuring Relays and Protection Equipment-Part 1: Common requirements, IEC 60255-1:2022, 2022.

[6] Technical Specifications of Handheld Optical Digital Signal Test Equipment in Smart Substation, DL/T 1944-2018, 2018.

[7] Technical Specifications of Digital Test Equipment for Relay Protection, DL/T 1501-2016, 2016.

[8] Technical Specifications for Digital-Analog Integrated Test Equipment for Relay Protection, DL/T 2646-2023, 2023.

[9] Calibration Specification Of Digital Signal Test Device for Intelligent Substation, NB/T 11216-2023, 2023.

[10] B. Zhang, Z. Hao, and Z. Bo, "New development in relay protection for smart grid," *Protection and Control*

*of Modern Power Systems*, vol. 1, no. 2, pp. 1-7, Apr. 2016.

[11] G. Chen, P. Wang, and Y. Zhao *et al.*, "Automatic test equipment design of intelligent terminals in a smart substation," *Power System Protection and Control*, vol. 49, no. 17, pp. 162-169, Sep. 2021. (in Chinese)

[12] Z. Li, J. Xu, and K. Wang *et al.*, "FPGA-based real-time simulation for EV station with multiple high-frequency chargers based on C-EMTP algorithm," *Protection and Control of Modern Power Systems*, vol. 5, no. 4, pp. 1-11, Oct. 2020.

[13] D. Omar, G. Ahmed, and O. Hamid *et al.*, "Comparison study of hardware architectures performance between FPGA and DSP processors for implementing digital signal processing algorithms:application of FIR digital filter," *Results in Engineering*, vol. 16, Dec. 2022.

[14] Y. Wang, Y. Liu, and M. Wang *et al.*, "Resilient smart power grid synchronization estimation method for system resilience with partial missing measurements," *CSEE Journal of Power and Energy Systems*, vol. 10, no. 3, pp. 1307-1319, Jul. 2024.

[15] Z. Gao, S. Gao, and Y. Yao *et al.*, "Systematic reliability evaluation of FPGA implemented CNN accelerators," *IEEE Transactions on Device and Materials Reliability*, vol. 23, no. 1, pp. 116-126, Mar. 2023.

[16] G. Zhang, J. Wang, and J. Guo *et al.*, "A novel single-DoF deployable antenna mechanism based on heterogeneous modules: configuration design and performance analysis," *Thin-Walled Structures*, vol. 203, Oct. 2024.

[17] O. Alberto, M. Asier, and M. D. A. Iñigo *et al.*, "Hardware design of a high-current, high step-down ratio series capacitor buck converter prototype for slow-ramped powering of high-luminosity large hadron collider inner triplet superconducting electromagnets," *Applied Energy*, vol. 371, Oct. 2024.

[18] Z. Zhang, T. Shi, and L. Lombardo *et al.*, "A fast self-calibration method for piezoelectric sensors excited by pseudorandom M-sequence," *IEEE Transactions on Instrumentation and Measurement*, vol. 73, pp. 1-9, Aug. 2024.

[19] M. T. V. Martinez, M. P. Comech, and A. A. P. Hurtado *et al.*, "Software-defined analog processing based on IEC 61850 implemented in an edge hardware platform to be used in digital substations," *IEEE Access*, vol. 12, pp. 11549-11560, Jan. 2024.

[20] M. M. Wong, D. M. L. Wong, and C. Zhang *et al.*, "Circuit and system design for optimal lightweight AES encryption on FPGA," *IAENG International Journal of Computer Science*, vol. 45, no. 1, pp. 136-146, Feb. 2018.

[21] A. Messai, I. Abdellani, and A. Mellit, "FPGA-based real-time implementation of a digital reactivity-meter," *Progress in Nuclear Energy*, vol. 150, Aug. 2022.

[22] M. H. Elkholy, H. Metwally, and M. A. Farahat *et al.*, "Smart centralized energy management system for autonomous microgrid using FPGA," *Applied Energy*, vol. 317, Jul. 2022.

[23] J. Yang, H. Lin, and H. Zhu *et al.*, "FPGA-based digital implementation of flexible power control for three-phase to single-phase MMC-based advanced co-phase traction power supply system," *Journal of Modern Power Systems and Clean Energy*, vol. 11, no. 6, pp. 2015-2027, May 2023.

[24] L. Chen, X. Wang, and W. Jin *et al.*, "Point-to-point intensity modulation and direct detection flexible transceivers incorporating cascaded inverse fast Fourier transform/fast Fourier transform-based multi-channel aggregation/de-aggregation techniques" *IET Optoelectronics*, vol. 18, no. 1-2, pp. 41-47, Feb. 2024.

[25] B. Sun, X. Wu, and X. Chen *et al.*, "Parameter estimation of sub-/super-synchronous oscillation based on interpolated all-phase fast Fourier transform with optimized window function," *Journal of Modern Power Systems and Clean Energy*, vol. 12, no. 4, pp. 1031-1041, Jul. 2024.

[26] H. Liu, F. Hu, and J. Su *et al.*, "Comparisons on Kalman-Filter-based dynamic state estimation algorithms of power systems," *IEEE Access*, vol. 8, pp. 51035-51043, Mar. 2020.

[27] K. Kim and J. H. Kim, "Polynomial regression predistortion for phase error calibration in X-band SAR," *IEEE Geoscience and Remote Sensing Letters*, vol. 19, pp. 1-5, Oct. 2020.

[28] Y. Wang, R. Chen, and Y. Yang, "Harmonic and inter-harmonic detection algorithm based on improved TLS-ESPRIT and a self-convolution window," *Power System Protection and Control*, vol. 51, no. 17, pp. 159-168, Sep. 2023. (in Chinese)

[29] Z. Yao, D. Li, and Z. Li *et al.*, "Relay protection mirror operation technology based on digital twin," *Protection and Control of Modern Power Systems*, vol. 8, no. 4, pp. 1-14, Oct. 2023.

[30] J. Bai, S. Huo, and A. Duffy *et al.*, "Improvement of nonembedded EMC uncertainty analysis methods based on data fusion technique," *IEEE Transactions on Electromagnetic Compatibility*, vol. 66, no. 6, pp. 1999-2009, Dec. 2024.